

gulate and SMA regions, activation in these regions was less significant during replay because of greater intersubject variability. Foci of maximal activation during replay included  $x = -6$ ,  $y = 9$ ,  $z = 45$  ( $Z = 4.69$ ;  $P = 0.06$  corrected) and  $x = 6$ ,  $y = 18$ ,  $z = 48$  ( $Z = 4.56$ ;  $P = 0.1$  corrected).

17. G. F. Poggio, F. Gonzalez, F. Krause, *J. Neurosci.* **8**, 4531 (1988); F. Sengpiel and C. Blakemore, *Nature* **368**, 847 (1994).

18. Superior parietal activity has not been observed during the performance of difficult visual tasks that do not involve spatial shifts of attention [M. Corbetta, F. M. Miezin, S. Dornmeyer, G. L. Shulman, S. E. Petersen, *J. Neurosci.* **8**, 2383 (1991); H. J. Heinze et al., *Nature* **372**, 543 (1995); M. Corbetta, G. L. Shulman, F. M.

Miezin, S. E. Petersen, *Science* **270**, 802 (1995); G. Rees, C. D. Frith, N. Lavie, *ibid.* **278**, 1616 (1997).

19. For reviews on modulation of activity by attention in ventral visual pathways, see R. Desimone and J. Duncan, *Annu. Rev. Neurosci.* **18**, 193 (1995); J. H. R. Maunsell, *Science* **270**, 764 (1995).

20. S. M. Courtney, L. G. Ungerleider, K. Keil, J. M. Haxby, *Nature* **386**, 608 (1997); S. P. O. Scalaidhe, F. A. W. Wilson, P. S. Goldman-Rakic, *Science* **278** (1997).

21. K. M. Heilman and T. Van Den Abell, *Neurology* **30**, 327 (1980); M.-M. Mesulam, *Annals Neurol.* **10**, 309 (1981); M. Husain and C. Kennard, *J. Neurol.* **243**, 652 (1996).

22. M. Corbetta, F. M. Miezin, G. L. Shuman, S. E. Petersen, *J. Neurosci.* **13**, 1202 (1993); A.C. Nobre et

al., *Brain* **120**, 515 (1997).

23. G. R. Fink et al., *Nature* **382**, 626 (1996).

24. M. Corbetta, *Proc. Natl. Acad. Sci. U.S.A.* **95**, 831 (1998).

25. G. W. Humphreys, C. Romani, A. Olson, M. J. Rid-doch, J. Duncan, *Nature* **372**, 357 (1994); M. Husain, K. Shapiro, J. Martin, C. Kennard, *ibid.* **385**, 154 (1997).

26. We thank O. Josephs and C. Büchel for assistance, R. Turner for advice on fMRI, and T. Griffiths and R. Frackowiak for comments on the manuscript. This work was funded by the Wellcome Trust.

4 February 1998; accepted 15 May 1998

## Proton Transfer Pathways in Bacteriorhodopsin at 2.3 Angstrom Resolution

Hartmut Luecke,\* Hans-Thomas Richter, Janos K. Lanyi\*

Photoisomerization of the retinal of bacteriorhodopsin initiates a cyclic reaction in which a proton is translocated across the membrane. Studies of this protein promise a better understanding of how ion pumps function. Together with a large amount of spectroscopic and mutational data, the atomic structure of bacteriorhodopsin, determined in the last decade at increasing resolutions, has suggested plausible but often contradictory mechanisms. X-ray diffraction of bacteriorhodopsin crystals grown in cubic lipid phase revealed unexpected two-fold symmetries that indicate merohedral twinning along the crystallographic  $c$  axis. The structure, refined to 2.3 angstroms taking this twinning into account, is different from earlier models, including that most recently reported. One of the carboxyl oxygen atoms of the proton acceptor Asp<sup>85</sup> is connected to the proton donor, the retinal Schiff base, through a hydrogen-bonded water and forms a second hydrogen bond with another water. The other carboxyl oxygen atom of Asp<sup>85</sup> accepts a hydrogen bond from Thr<sup>89</sup>. This structure forms the active site. The nearby Arg<sup>82</sup> is the center of a network of numerous hydrogen-bonded residues and an ordered water molecule. This network defines the pathway of the proton from the buried Schiff base to the extracellular surface.

ing values:  $R$  factor, 18.0%;  $R_{\text{free}}$ , 23.6%; and average  $B$ , 26.7 Å<sup>2</sup>. More detailed statistical information is given in Table 1.

The overall seven-helical structure is similar to those previously determined (3–5). The loop between helices B and C forms a short antiparallel  $\beta$ -sheet in the same orientation as in the electron diffraction structures (3, 4). We observed no density for residues 1 to 5, 154 to 166 (the loop between helices E and F), and 229 to 248 (COOH-terminus). In several positions equivalent to the diacyl lipid positions observed in one of the earlier structures from electron diffraction (3), we also observed long sections of density with various branch points that we interpret as native dihydrophytyl lipids, carried along through solubilization and cubic lipid phase crystallization. Model building and refinement for these areas are in progress.

The densities and the refined model at locations of interest are shown in Fig. 2. The immediate environment of the retinal Schiff base is shown in Fig. 2A. OD1 of Asp<sup>85</sup>, the proton acceptor from the Schiff base in the transport cycle, is hydrogen-bonded to a water molecule, labeled W401 (8). OD1 of Asp<sup>85</sup> also accepts a hydrogen bond from another water molecule (W402) that in turn accepts a hydrogen bond from the Schiff base, a feature predicted and much discussed (9) but not detected before. This water molecule and Thr<sup>89</sup>, which is hydrogen-bonded to OD2 of Asp<sup>85</sup> (see below), should together lower the  $pK_a$  ( $K_a$  is the acid dissociation constant) of Asp<sup>85</sup> and thereby stabilize the otherwise energetically unfavorable Schiff base–Asp<sup>85</sup> ion pair in the unphotolyzed protein. If the two hydrogen bond donors were displaced or entered into hydrogen-bonding with other partners after photoisomerization of the retinal, the  $pK_a$  of Asp<sup>85</sup> would be raised, and this would be a reason for its protonation by the Schiff base.

The extracellular region where proton release to the surface is induced by protonation of Asp<sup>85</sup> (10) is shown in Fig. 2B. Because titration of Asp<sup>85</sup> in the dark detects the dependence of its  $pK_a$  on the

**B**acteriorhodopsin is a small integral membrane protein that functions as a light-driven proton pump (1). Its seven-helical structure has been described (2–5) at increasing resolutions, most recently at 2.5 Å. The protein crystallizes from cubic lipid phase as thin hexagonal plates containing stacked layers of two-dimensional sheets of trimers, similar to the naturally occurring two-dimensional lattice formed by bacteriorhodopsin (5, 6). The time courses of absorbance changes at 570, 410, and 640 nm after flash photoexcitation (7) indicate that the photochemical cycle in these crystals is nearly equivalent to that of purple membrane suspensions. We measured x-ray diffraction from these crystals. They belong to space group  $P6_3$  with two trimers per unit

cell, offset by  $\frac{1}{2}$  in  $c$ . In addition to the expected sixfold symmetry along the  $c$  axis, there are, unexpectedly, additional twofold axes in the  $a/b$  plane, as shown in Fig. 1. Given the space group for these crystals, this is an indication of merohedral twinning, a phenomenon not uncommon for certain space groups. Twinned crystals require special consideration because they are a mixture of two or more single crystals. If the twinning in these crystals were ignored, nearly 50% of the scattering matter would not be accounted for.

Taking twinning properly into account yielded a refined structure different in some respects from the one that first used crystals from cubic lipid phase (5). Also, the statistics of the refinement as well as the electron density maps are improved. The previously reported  $R$  factor and  $R_{\text{free}}$  were 22.1% and 32.7%, respectively, for data with  $F > 3\sigma(F)$  between 2.5 and 5.0 Å, with an unusually high average  $B$  factor of 54 Å<sup>2</sup> (5). Calculating these parameters in the same way (omitting data higher than 5 Å), but not using a  $\sigma$ -based cutoff, we found the follow-

H. Luecke, Department of Molecular Biology and Biochemistry and Department of Physiology and Biophysics, University of California, Irvine, CA 92697, USA.  
H.-T. Richter and J. K. Lanyi, Department of Physiology and Biophysics, University of California, Irvine, CA 92697, USA.

\*To whom correspondence should be addressed. E-mail: HUDEL@UCI.EDU or JLANYI@ORION.OAC.UCI.EDU

proton occupancy of the proton release chain, the pathway of the released proton should be evident in the unphotolyzed protein. Indeed, there are strong clues in this structure. The NE of Arg<sup>82</sup> is hydrogen-bonded to a water molecule (W403), which is at hydrogen-bonding distance (at a some-

what long 3.5 Å) from OE2 of Glu<sup>204</sup>. This carboxyl oxygen is within 4.0 Å of OE2 of Glu<sup>194</sup> and thus provides a possible pathway for the released proton. Two unassigned disconnected densities in this region (one shown as W in Fig. 2B) are likely to be additional water molecules that could par-

ticipate in proton conduction, but their distances from protein residues appear to be slightly longer than hydrogen bonds. The suggested alternative pathway (5) that passes through Thr<sup>205</sup> and Glu<sup>9</sup> has somewhat less favorable distances and orientation, and water is not detected in that region. Indeed, extensive mutational and spectroscopic studies (11–13) have indicated that Arg<sup>82</sup>, Glu<sup>204</sup>, and Glu<sup>194</sup> constitute the pathway of the released proton, whereas Glu<sup>9</sup> and Thr<sup>205</sup> can be replaced without affecting proton release (13). Although some evidence suggests it, the small amplitude (12) of the depletion peak of the C=O stretch band of protonated Glu<sup>204</sup> (and Asp<sup>204</sup> in the Glu<sup>204</sup> → Asp mutant) makes it doubtful that the origin of the released proton is the COOH of Glu<sup>204</sup>. It is evident from Fig. 2B, however, that water molecule W403 is a strong alternative candidate.

The polyene chain of the retinal and its surroundings are shown in Fig. 2C. The 9-methyl and 13-methyl groups are 3.6 to 3.7 Å from the closest heavy atom of Trp<sup>182</sup> and Leu<sup>93</sup>, respectively, consistent with evidence (14) that these residues are the contact points between the retinal and the protein that affect thermal reisomerization from 13-*cis* to all-*trans* near the end of the photocycle. The cytoplasmic region with Asp<sup>96</sup>, the proton donor to the unprotonated Schiff base after protonation of Asp<sup>85</sup> in the photocycle, is shown in Fig. 2D. Asp<sup>96</sup> is flanked by Phe<sup>42</sup> and Phe<sup>219</sup>. This and the generally hydrophobic environment of this region (2, 3) are consistent with the very high pK<sub>a</sub> observed (>11) for Asp<sup>96</sup> in the unphotolyzed protein (15).

**Fig. 1.** Patterson self-rotation function of structure factor set reduced in space group *P6*, contoured starting at 5σ in 1σ increments. The diagram shows the presence of a strong two-fold axis along the crystallographic *c* axis ( $\Psi = 90^\circ$ ,  $\varphi = 90^\circ$ ,  $\kappa = 180^\circ$ ) as expected for a crystallographic six-fold axis [prepared with GLRF (25)]. In addition, however, equally strong two-fold peaks occur every 30° in the *a/b* plane. These peaks are usually an indication of a space group of the 622 Laue family with 12 copies of the asymmetric unit per unit cell. Because the unit cell volume (*V*) of the crystals ( $a = b = 60.85$  Å,  $c = 108.4$  Å;  $V = 348,000$  Å<sup>3</sup>) only allows for six copies of the bacteriorhodopsin molecule (unit cell volume divided by unit cell molecular weight,  $V_M = 2.23$  Å<sup>3</sup>/D), these additional two-fold axes are a result of merohedral twinning along the crystallographic *c* axis (22). The twinning matrix relating one set of structure factors to their respective twin components is [0 1 0; 1 0 0; 0 0 -1]. Another indication of the nearly perfect merohedral twinning of these crystals is the fact that reducing the data in the higher symmetry space group *P622* only slightly increases the  $R_{\text{merge}}$  of the data set from 11.3% to 14.2%. A third indication is the fact that we obtained two solutions to the cross-rotation function with almost equal peak heights, related to each other by a 180° rotation in the *a/b* plane (see Table 1). All crystals examined exhibited close to 50:50 twinning, regardless of size.

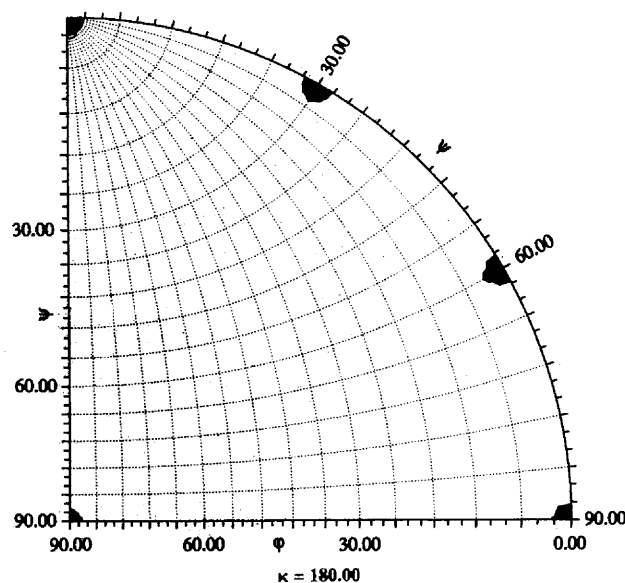
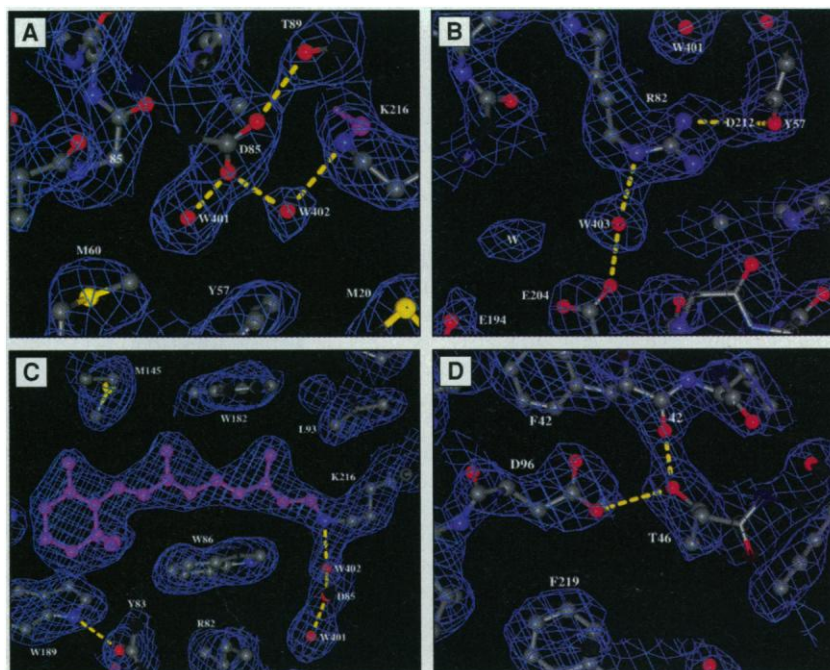


**Fig. 2.** Electron density maps ( $2|F_o| - |F_c|$ , contoured at 1σ) and corresponding molecular models of three regions of interest. Dashed yellow lines indicate hydrogen bonds. **(A)** The region of the Schiff base and the initial proton acceptor, Asp<sup>85</sup>. OD1 of Asp<sup>85</sup> is within hydrogen-bonding distance of a water molecule (W401,  $B = 3.1$  Å<sup>2</sup>) (7). Another water (W402,  $B = 24.7$  Å<sup>2</sup>) molecule was identified between the Schiff base and OD1 of Asp<sup>85</sup>. **(B)** Region between Arg<sup>82</sup> and Glu<sup>204</sup>. Water W403 ( $B = 23.8$  Å<sup>2</sup>) hydrogen-bonds to both NE of Arg<sup>82</sup> and OE1 of Glu<sup>204</sup> and is the potential source of the proton released to the surface when Asp<sup>85</sup> becomes protonated. The feature labeled as W is one of three disconnected densities in this immediate region. Although they are likely to be water, we did not model them because their ligand arrangement is uncertain at the present resolution. **(C)** Region of the retinal (magenta), showing residues Trp<sup>182</sup>, Leu<sup>93</sup>, Met<sup>145</sup>, and Trp<sup>86</sup>, which flank it. The OH of Tyr<sup>83</sup> forms a hydrogen bond with the indole N of Trp<sup>189</sup>. **(D)** Region near Asp<sup>96</sup> in the cytoplasmic portion of the proton translocation pathway. The hydroxyl of Thr<sup>46</sup> forms a hydrogen bond with the peptide C=O of Phe<sup>42</sup>. The distance between Asp<sup>96</sup> and the Thr<sup>46</sup> hydroxyl (drawn in) is 3.5 Å, which may be sufficient for a hydrogen bond. Single-letter abbreviations for the amino acid residues are as follows: D, Asp; E, Glu; F, Phe; L, Leu; M, Met; R, Arg; T, Thr; W, Trp; and Y, Tyr.



The Thr<sup>46</sup> hydroxyl is hydrogen-bonded to the peptide carbonyl of Phe<sup>42</sup> (2.7 Å), and its distance to Asp<sup>96</sup> at 3.5 Å may be consistent with a hydrogen bond. The observation that the Thr<sup>46</sup> → Val residue replacement makes protonation of the Schiff base by Asp<sup>96</sup> more rapid and reprotonation of Asp<sup>96</sup> much slower (16) suggests that even if they are not initially, Thr<sup>46</sup> and Asp<sup>96</sup> might become hydrogen-bonded during the photocycle. Remarkably, no ordered water is observed that would facilitate the transfer of a proton from Asp<sup>96</sup> to the Schiff base over the 12 Å distance between them.

From the structure, shown schematically in Fig. 3, it is evident that, although Asp<sup>212</sup> is close to W402 like Asp<sup>85</sup>, it is hydrogen-bonded differently. Hydrogen-bonding of its OD1 to Tyr<sup>57</sup> and OD2 to Tyr<sup>185</sup> and another hydrogen bond of OD1 to the NH<sub>2</sub> of Arg<sup>82</sup> form a three-dimensional hydrogen-bonded network that may account for the unusually low pK<sub>a</sub> of Asp<sup>212</sup> (<2). This may be why Asp<sup>212</sup> is not the proton acceptor of the Schiff base. The extended hydrogen-bonded structure, which includes an aspartate, an arginine, two tyrosines, and a water, is part of the diffuse counterion to the Schiff base evident from nuclear magnetic resonance (17). The structure suggests that the proton released to the extracellular surface is from water molecule W403 and the pathway is through Glu<sup>204</sup> and Glu<sup>194</sup>. Replacement of this proton from Asp<sup>85</sup> at the end of the photocycle must occur through rearranged hydrogen bonds that establish a chain of connection between Asp<sup>85</sup> and Arg<sup>82</sup>.

The three previously published structural models for bacteriorhodopsin and our model differ from one another. The largest differences are in the number and positions of hydrogen-bonded water molecules near the Schiff base and in the connectivities of residues in the extracellular region that determine the proton-conducting pathway to the membrane surface. Although all models connect Tyr<sup>57</sup>, Asp<sup>212</sup>, and Tyr<sup>185</sup> with hydrogen bonds (18), in the model of Grigorieff *et al.* (3), Trp<sup>86</sup> is also within hydrogen-bonding distance of Asp<sup>212</sup>. In the model of Kimura *et al.* (4), the retinal Schiff base is hydrogen-bonded to Asp<sup>212</sup>, and in the model of Pebay-Peyroula *et al.* (5), Asp<sup>85</sup> is hydrogen-bonded to Trp<sup>86</sup>. None of these additional hydrogen bonds appear in our model. Asp<sup>85</sup> is hydrogen-bonded to Thr<sup>89</sup> in all models except that of Kimura *et al.* (4). The side chain of Arg<sup>82</sup> points toward the extracellular surface in the model of Grigorieff *et al.* (3) but to various extents more toward the retinal Schiff base in the other models. Only in our model is there hydrogen-bonding between Arg<sup>82</sup> and Asp<sup>212</sup> (Fig. 2B), and only in this model are the retinal Schiff base and Asp<sup>85</sup> bridged by

a water molecule (Fig. 2, A and C). In the models of Grigorieff *et al.* (3) and Pebay-Peyroula *et al.* (5), the pathway of the proton release to the cytoplasmic surface is more likely to be through Thr<sup>205</sup> and Glu<sup>9</sup> than through Glu<sup>204</sup> and Glu<sup>194</sup>, because the distances are substantially shorter and the orientations more favorable. In the model of Kimura *et al.* (4) and our model,

the pathway through Glu<sup>204</sup> and Glu<sup>194</sup> is more likely, but proton transfer to the surface through Thr<sup>205</sup> and Glu<sup>9</sup> is not ruled out. In addition to the mutational and spectroscopic evidence cited above, the observation of a water molecule between Arg<sup>82</sup> and Glu<sup>204</sup>, which appears only in our structure (Fig. 2B), argues in favor of the proton pathway through Glu<sup>204</sup>. On the cytoplasmic

**Fig. 3.** Schematic of the active site and part of the extracellular proton translocation pathway. The distances of relevant groups (in angstroms) are as follows: Schiff base (NZ) to W402, 2.7; W402 to Asp<sup>85</sup> (OD1), 2.8; W402 to Asp<sup>212</sup> (OD1), 3.4; W402 to Asp<sup>212</sup> (OD2), 3.6; Asp<sup>85</sup> (OD1) to W401, 2.6; Asp<sup>85</sup> (OD2) to Thr<sup>89</sup> (OH), 2.7; Arg<sup>82</sup> (NH<sub>2</sub>) to Asp<sup>212</sup> (OD1), 3.3; Asp<sup>212</sup> (OD1) to Tyr<sup>57</sup> (OH), 2.8; Asp<sup>212</sup> (OD2) to Tyr<sup>185</sup>, 2.6; Arg<sup>82</sup> (NE) to W403, 3.2; W403 to Glu<sup>204</sup> (OE2), 3.5; Arg<sup>82</sup> (NH<sub>2</sub>) to W401, 4.2; Asp<sup>212</sup> (OD1) to W401, 4.9; and Tyr<sup>57</sup> (OH) to W401, 5.1.

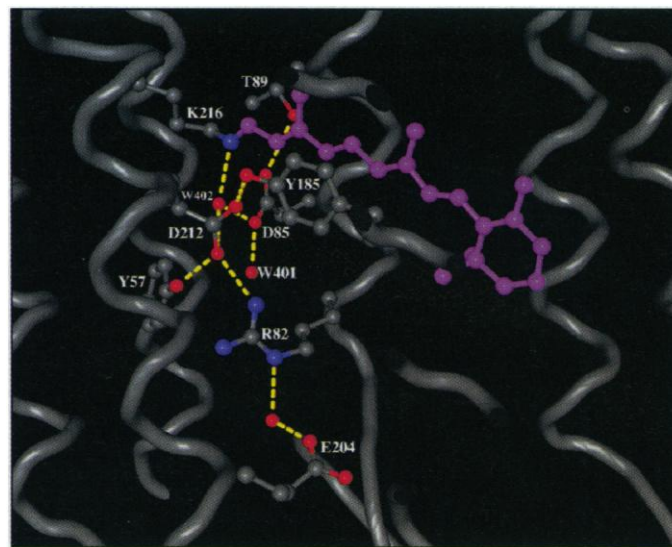


**Fig. 4.** Ribbon stereo diagram of bacteriorhodopsin molecule showing the location of two internal cavities, prepared with GRASP (26) with a 1.4 Å probe radius. The seven transmembrane helices shown are roughly normal to the plane of the bilayer. The cytoplasmic side is the top. The larger, irregularly shaped cavity (80 Å<sup>3</sup>, blue) is located between Arg<sup>82</sup>, Glu<sup>204</sup>, and Glu<sup>194</sup> in the extracellular portion of the proton translocation pathway, and its largest dimension measures about 6 Å. Difference density maps indicated the presence of water molecules in this area, one of which is W403 (Fig. 2B) and is included in the model. The smaller cavity (20 Å<sup>3</sup>, red) is located in a hydrophobic region between the Schiff base and Asp<sup>96</sup> in the cytoplasmic portion of the proton translocation pathway. No substantial difference density features were observed in this area. This smaller volume could accommodate only one or two disordered water molecules without conformational changes.

mic side, the proximity of Asp<sup>96</sup> to Phe<sup>42</sup> that we found (Fig. 2D) is in the models of Grigorieff *et al.* (3) and Pebay-Peyroula *et al.* (5) but not in the model of Kimura *et al.* (4). Substantial and numerous differences exist also between the two electron microscopy (EM) structures in the positions of other side chains near the surfaces, as pointed out recently by Kimura *et al.* (19).

The scarcity of liganded water in the protein interior is a surprise, as in the earlier structure (5). Unordered water cannot be

detected but may be deduced from cavities inside the protein (3). As shown in Fig. 4, two cavities of substantial size were found. The larger cavity is in the region of Arg<sup>82</sup>, Glu<sup>204</sup>, and Glu<sup>194</sup>. It may contain as many as three to four water molecules and lends support to the suggestion that proton release is through Glu<sup>194</sup>. The smaller cavity is between Asp<sup>96</sup> and the Schiff base. It could contain one to two water molecules, which possibly have a role in the reprotonation of the Schiff base if they shuttle protons or

become organized to form a hydrogen-bonded chain, during the photocycle. In the earlier electron diffraction structure (3), the same kind of search turned up as many as 12 cavities that could contain at least one water molecule. The structure we describe here shows considerably fewer potential sites for disordered water molecules.

REFERENCES AND NOTES

1. R. A. Mathies, S. W. Lin, J. B. Ames, W. T. Pollard, *Ann. Rev. Biophys. Biophys. Chem.* **20**, 491 (1991); J. K. Lanyi, *Biochim. Biophys. Acta* **1183**, 241 (1993).
2. R. Henderson *et al.*, *J. Mol. Biol.* **213**, 899 (1990).
3. N. Grigorieff, T. A. Ceska, K. H. Downing, J. M. Baldwin, R. Henderson, *ibid.* **259**, 393 (1996).
4. Y. Kimura *et al.*, *Nature* **389**, 206 (1997).
5. E. Pebay-Peyroula, G. Rummel, J. P. Rosenbusch, E. M. Landau, *Science* **277**, 1676 (1997).
6. E. M. Landau and J. P. Rosenbusch, *Proc. Natl. Acad. Sci. U.S.A.* **93**, 14532 (1996).
7. H. Luecke, H.-T. Richter, J. K. Lanyi, data not shown.
8. Relative to the neighboring atoms, W401 has an unusually low B factor. However, because in a preliminary model from a new data set with higher resolution this B factor appears more normal, we modeled this density as a water molecule.
9. F. Zhou, A. Windemuth, K. Schulten, *Biochemistry* **32**, 2291 (1993); Y. Gat and M. A. Sheves, *J. Am. Chem. Soc.* **115**, 3772 (1993); B. Roux, M. Nina, R. Pomès, J. C. Smith, *Biophys. J.* **71**, 670 (1996).
10. S. P. Balashov, E. S. Imasheva, R. Govindjee, T. G. Ebrey, *Biophys. J.* **70**, 473 (1996); H.-T. Richter, L. S. Brown, R. Needleman, J. K. Lanyi, *Biochemistry* **35**, 4054 (1996).
11. S. P. Balashov *et al.*, *Biochemistry* **32**, 10331 (1993); S. P. Balashov *et al.*, *ibid.* **36**, 8671 (1997).
12. L. S. Brown *et al.*, *J. Biol. Chem.* **270**, 27122 (1995).
13. A. K. Dioumaev *et al.*, *Biochemistry* **37**, 2496 (1998). The phenotype of the Thr<sup>205</sup> → Val mutant is from L. S. Brown and J. K. Lanyi (unpublished results).
14. Y. Yamazaki *et al.*, *Biophys. J.* **34**, 577 (1995); O. Weidlich *et al.*, *ibid.* **35**, 10807 (1996); J. K. Delaney, U. Schweiger, S. Subramaniam, *Proc. Natl. Acad. Sci. U.S.A.* **92**, 11120 (1995).
15. S. Szárás, D. Oesterhelt, P. Ormos, *Biophys. J.* **67**, 1706 (1994).
16. T. Marti *et al.*, *J. Biol. Chem.* **266**, 6919 (1991); L. S. Brown *et al.*, *J. Mol. Biol.* **239**, 401 (1994).
17. H. J. M. De Groot, G. S. Harbison, J. Herzfeld, R. G. Griffin, *Biochemistry* **28**, 3346 (1989).
18. Hydrogen bonds are inferred from interatomic distances.
19. Y. Kimura *et al.*, *Photochem. Photobiol.* **66**, 764 (1997).
20. Z. Otwinowski, in *Data Collection and Processing*, L. Sawyer, N. Isaacs, S. Bailey, Eds. (SERC Daresbury Laboratory, Warrington, UK, 1993), pp. 56–62.
21. A. T. Brünger, *X-PLOR, Version 3.1: A System for X-Ray Crystallography and NMR* (Yale Univ. Press, New Haven, CT, 1992).
22. G. M. Sheldrick and T. Schneider, *Methods Enzymol.* **277**, 319 (1997).
23. More details about twinning of cubic lipid phase bacteriorhodopsin crystals can be found at <http://anx12.bio.uci.edu/~hucel/br/twinning/index.html>.
24. M. R. Redinbo and T. O. Yeates, *Acta Crystallogr. D* **49**, 375 (1993).
25. L. Tong and M. G. Rossman, *Acta Crystallogr. A* **46**, 783 (1990).
26. A. Nicholls, K. A. Sharp, B. Honig, *Proteins* **11**, 281 (1991).
27. We thank Y. Kimura and E. Pebay-Peyroula for making their coordinates available and E. Pohl and A. McPherson for comments on twinning. Supported in part by grants from NIH to H.L. (R01-GM56445) and J.K.L. (R01-GM29498) and from the U.S. Department of Energy to J.K.L. (DEFG03-86ER13525). The coordinates of the structure in this paper have been deposited in the Brookhaven Protein Data Bank (entry code 1BRX).

26 January 1998; accepted 7 May 1998

**Table 1.** X-ray data collection, molecular replacement, and refinement statistics. Crystals were grown as described previously (6) and form thin hexagonal plates typically about 80 μm × 80 μm × 15 μm. Diffraction data were collected on light-adapted, cryo-cooled crystals with a Rigaku RU3 generator with mirror focusing optics, with a Rigaku R-Axis IV imaging plate detector. Each image was 1° in φ with an exposure time of 15 min. Images were reduced, scaled, and merged with the programs DENZO and SCALEPACK (20). Molecular replacement was carried out with the program X-PLOR (21). The use of either the EM structure of Grigorieff *et al.* (3) (2BRD) or that of Kimura *et al.* (4) (1APT) resulted in two cross-rotation function peaks of nearly equal magnitude (peak 1: [0.0°, 0.0°, 0.0°], height 5.44; peak 2: [0.0°, 180.0°, 0.0°], height 5.18; first noise peak height 4.43), related to each other by a 180° rotation in the a/b plane, a direct result of crystal twinning. The translation function gave a clear solution for [0.333, 0.667, 0], attesting to the similarity between the P3 electron microscopy crystal lattice and the P6<sub>3</sub> three-dimensional crystal lattice. The presence of merohedral twinning made the program SHELXL-97 (22) the obvious choice for crystallographic refinement. If the twinning were neglected, one would be refining the model against structure factors that have contributions from both twin components (23). Refinement of a twinned structure introduces only one additional parameter that describes the relative twin fractions. For the R<sub>free</sub> test, 5% of all structure factors were set aside in such a way that all structure factors in each of several thin resolution shells were selected to avoid bias due to the presence of the twinning operator. The first round of refinement (with all data but without a σ cutoff) consisted of 20 cycles of conjugate gradient minimization with a gradual extension of the resolution from 3.3 to 2.3 Å with highly restrained geometries and temperature factors and resulted in an R factor of 27.4% and an R<sub>free</sub> of 34.4%. In contrast, use of the same refinement protocol without accounting for twinning resulted in an R factor of 36.8% and an R<sub>free</sub> of 43.4%. In the initial stages of refinement, the side chain atoms of key residues such as the retinal, Asp<sup>85</sup>, Asp<sup>212</sup>, Arg<sup>82</sup>, Glu<sup>204</sup>, Thr<sup>89</sup>, Tyr<sup>57</sup>, Tyr<sup>185</sup>, Trp<sup>96</sup>, Trp<sup>182</sup>, Met<sup>60</sup>, and Asp<sup>96</sup> of the EM model used (4) were omitted to minimize model bias. These side chains were manually built into 3|F<sub>o</sub> - 2|F<sub>c</sub>| omit maps. Several rounds of manual model improvement followed by refinement resulted in an R factor of 18.0% and an R<sub>free</sub> of 26.6%. For statistical reasons, the R factor for merohedrally twinned data can be up to 1.4 times lower than for an equivalent nontwinned case, assuming a random atom distribution (24). All peptide bonds fall into the allowed regions of the Ramachandran plot.

	Data reduction resolution range	
	2.3–25.0 Å	2.30–2.34 Å
Total observations	250,474	
Unique structure factors*	9,769	
R <sub>merge</sub> (I) (%)†	11.3	44.3
Average I/σ(I)‡	15.1	1.7
Completeness (%)	96.5	75.9
Mosaicity (°)	0.72	
Refinement resolution range 2.3–12.0 Å		
Number of structure factors*	9,696	
Number of restraints	6,912	
Number of parameters	6,544	
Twin ratio	0.54:0.46	
Number of protein atoms	1,612	
Number of retinal atoms	20	
Number of solvent molecules	3	
R factor§ (%) for all data	22.3	
R factor (%) for data with F > 4σ(F)	18.0	
R <sub>free</sub> (I) (%)	26.6	
Average protein B (Å <sup>2</sup> )	25.2	
Average retinal B (Å <sup>2</sup> )	16.9	
Deviation from ideal bond lengths (Å)	0.014	
Deviation from ideal bond angles (°)	1.653	

\*The presence of twinning introduces some degree of redundancy. † $R_{merge}(I) = \sum_{hkl} \sum_i |I_{hkl,i} - \langle I_{hkl} \rangle| / \sum_{hkl} \sum_i I_{hkl,i}$ , where  $\langle I_{hkl} \rangle$  is the average intensity of the multiple  $I_{hkl,i}$  observations for symmetry-related reflections. ‡ $I/\sigma(I)$ , average of the diffraction intensities, divided by their standard deviations. §R factor =  $\sum_{hkl} |F_o - F_c| / \sum_{hkl} |F_o|$ , where  $F_o$  and  $F_c$  are observed and calculated structure factors, respectively. ¶ $R_{free} = \sum_{hkl \in T} |F_o - F_c| / \sum_{hkl \in T} |F_o|$ , where the T set (5% of the data) is omitted from the refinement.